A Journal of the Gesellschaft Deutscher Chemiker

Angewandte International Edition GDCh Chemie

www.angewandte.org

Accepted Article

Title: Shaping microcrystals of metal-organic frameworks by reaction-diffusion

Authors: Jun Heuk Park, Jan Paczesny, Namhun Kim, and Bartosz Grzybowski

To be cited as: *Angew. Chem. Int. Ed.* 10.1002/anie.201910989
Angew. Chem. 10.1002/ange.201910989

Link to VoR: http://dx.doi.org/10.1002/anie.201910989
http://dx.doi.org/10.1002/ange.201910989

WILEY-VCH

Angewandte Chemie International Edition
Angewandte Communications
10.1002/anie.201910989

Reaction-Diffusion

DOI: 10.1002/anie.201((will be filled in by the editorial staff))

Shaping microcrystals of Metal-Organic Frameworks by Reaction-Diffusion **

*Jun Heuk Park, Jan Paczesny, Namhun Kim, Bartosz A. Grzybowski**

Abstract. *When components of a metal organic framework, MOF, and a crystal growth modulator diffuse through a gel medium, they can form arrays of regularly-spaced precipitation bands containing MOF crystals of different morphologies. With time, slow variations in the local concentrations of the growth modulator cause the crystals to change their shapes, ultimately resulting in unusual concave microcrystallites not available via solution-based methods. The reaction-diffusion and periodic precipitation phenomena (i) extend to various types of MOFs and also MOPs (metal organic polyhedra), and (ii) can be multiplexed to realize within one gel multiple growth conditions, in effect leading to various crystalline phases or polycrystalline formations.*

Reaction diffusion, RD, systems – in which chemical reactions couple non-linearly with diffusive transport – have been studied for well over a century and in various contexts: from oscillating reactions, to systems chemistry, to micro- and nanofabrication, to cell biology[1]. One of the classic manifestations of RD has been the so-called periodic precipitation, PP,[2] in which reacting species diffusing though a porous matrix (usually a gel) form an array of distinct and regularly spaced precipitation bands (a.k.a. Liesegang rings[1a]). PP phenomena attracted considerable attention as a model system to study nonlinear chemical dynamics,[2b-d] and also for their relevance to the formation of patterns in minerals,[2e] or as a means of fabricating micro- and nanoarchitectures, including optical elements[1b,2d,f]. Although many types of PP systems have been demonstrated on scales from macro-[3a-c] through micro-[3d-f] to nanoscopic,[3g-i] virtually all of them are based on very rapid precipitation of inorganic ions or ionic nanoparticles[3j] leading to ill-shaped deposits. It has only been recently that Al-Ghoul and Hmadeh showed that periodic banding can also apply to metal-organic frameworks, MOFs. In particular, these authors demonstrated[4a] that diffusion of methylimidazole (outer electrolyte) through a gel column filled with $ZnSO_4$ or $CoSO_4$ (inner electrolytes) leads to the emergence of discrete precipitation zones containing ZIF-8 or ZIF-67 microcrystals. The sizes of these microcrystals increased with band number (as in the related works by the same authors where gradient crystallization of MOFs in gel was studied[4b-d]) but their morphologies did not change, save formation of holes in crystal faces. In the current work, we wished to combine such PP phenomena with the control the diffusive fluxes during RD such as to shape the emerging structures – we previously demonstrated similar control at the macroscale, in etching macroscopic structures made of metal nanoparticles.[5] Here, we wished to achieve it at smaller scales to control the habits and face curvatures of MOF crystals collecting in different periodic precipitation bands – we were interested in this problem both from a fundamental perspective (can RD be precise enough to separate differently-shaped crystals to different bands and then controllably "etch" them?) and also because some of the MOF

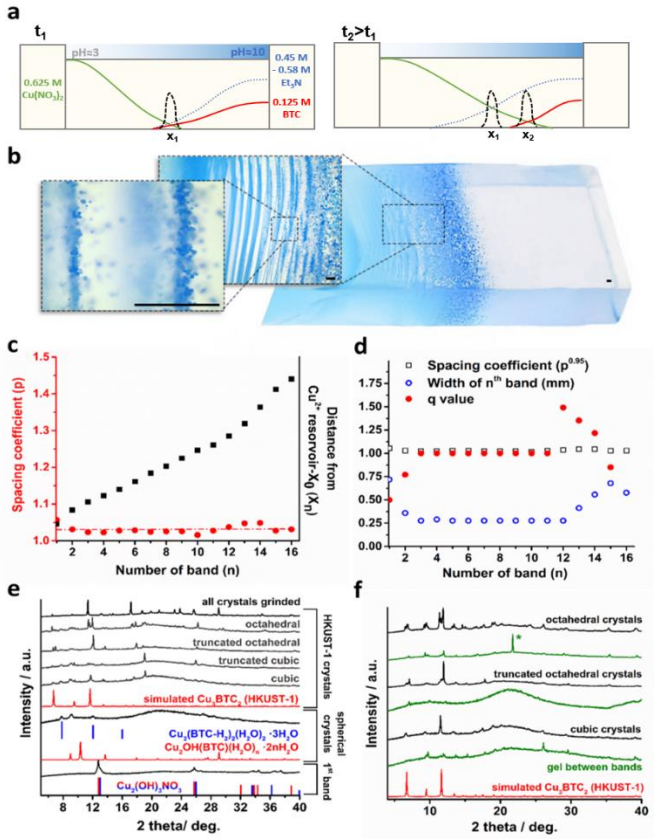

Figure 1. **(a)** Scheme of the basic experimental arrangement and qualitative concentration profiles of $Cu(NO_3)_2 \cdot 3H_2O$ (green curve), BTC/trimesic acid struts (red), and triethylamine (dotted blue) diffusing through the gel to produce periodic bands (black) of HKUST-1 MOF crystals. Scale above the gel indicates the pH gradient. **(b)** Optical images of PP patterns of HKUST-1 crystals shown at three different magnifications. Scale bars = 500 μm. **(c)** Distances of the PP bands from the Cu^{2+} reservoir (black markers) and calculated spacing coefficient, p (red markers). **(d)** Corresponding widths, w_n, of the bands (open blue markers) and calculated q values (red markers). Open black markers trace the expected phenomenological dependence, $q = p^k$ (k = 0.95). **(e)** PXRD spectra of material collected from slices of the gel corresponding to PP bands. Black = experimental spectra; red and blue = calculated spectra (see main text and SI, **Section S2**). **(f)** PXRD patterns for consecutive PP bands containing HKUST-1 crystals (black curves) and "empty" spaces between these bands (green curves). Between the PP bands, only some residues are present with exception of a strong peak marked with an asterisk and corresponding to $Cu(OH)_2$ (JCPDS#13-0420) formed at high concentration of Et_3N (i.e., at high pH).

[*] Dr. Jun Heuk Park, Dr. Jan Paczesny, Mr. Namhun Kim, Prof. B.A. Grzybowski
IBS Center for Soft and Living Matter and
Department of Chemistry, UNIST,
50, UNIST-gil, Eonyang-eup, Ulju-gun, Ulsan, South Korea
E-mail: nanogrzybowski@gmail.com

[**] Authors gratefully acknowledge generous support from the Institute for Basic Science Korea, Project Code IBS-R020-D1.

Supporting information for this article is available on the WWW under http://dx.doi.org/10.1002/anie.201xxxxxx.

10.1002/anie.201910989

applications[6a] can benefit from the control of crystals' habits (e.g., size[6b] and shape[6c] control of selective CO_2 capture). As we show, such control is indeed possible by diffusing through the supporting gel not only the components of the MOF but, simultaneously, also crystal-growth modulators. Under these conditions, the PP bands contain MOF crystals of different polyhedral habits which, remarkably, evolve in time to produce unusual concave structures that would be hard, if not impossible, to obtain via solution based methods. The Wet-Stamping[1b,3f,g,i] method enabling such controllable outcomes is applicable to various types of MOF and also metal-organic polyhedra (MOP), and can be multiplexed to screen crystal growth in multiple RD processes taking place simultaneously within the same gel.

As a model system, we chose popular HKUST-1 (MOF-199; $Cu_3(BTC)_2$, BTC=1,3,5-benzenetricarboxylate, a.k.a. trimesic acid) whose crystals are stable in aqueous media and thus in hydrogels commonly used for PP. The basic experimental setup is illustrated in **Figure 1a** and comprises a 18 x 6 x 3 mm^3 or 9 x 3 x 1.5 cm^3 column of 4% wt. agarose gel flanked by two 4 % w/w agarose gel reservoirs (respectively, 8 x 7 x 2.5 mm^3 or 4 x 3.5 x 1.5 cm^3) soaked with solutions of the MOFs components. This modality of Wet-Stamping[1b,3f,g,i] is used because it allows for controllable/diffusive transport between the gels which, compared to delivery from solution, suppresses any turbid flows and minimizes the so-called turbulent zone obscuring well-developed PP bands (**Figure 1b**). Unlike in most PP studies based on two reacting species, our system involves three – in one gel reservoir Cu^{2+} ions ($Cu(NO_3)_2{\cdot}3H_2O$) and in the other, the organic linker (BTC for HKUST-1) and triethylamine, Et_3N, which acts as deprotonating agent as well as a modulator accelerating nucleation and also capping specific crystal faces.[7] For best results, the concentration of copper ions has to be higher than that of BTC struts (typically, 0.625 M : 0.125 M), and the concentration of deprotonating agent (Et_3N) must be carefully controlled at 0.45 M (3.58 mmol in 8 mL of 1:1 v/v H_2O/EtOH mixture). Lower Et_3N concentrations give less or no crystal nucleation, while excess amount results in rapid deprotonation of BTC, translating into continuous gradient of crystals of different sizes rather than periodic precipitation. As these species diffuse from opposite directions, they "meet" near the center of the gel column where their relative concentration gradually increases and ultimately exceeds supersaturation threshold resulting in the formation of the first precipitation band (**Figure 1a**, *left*). The depleted reacting partners are resupplied by diffusion and supersaturation is reached again, albeit at a different location (typically on the side closer to the linker/modulator reservoir), to produce the second precipitation band (**Figure 1a**, *right*). The process then cyclically repeats and up to16 bands can be resolved (**Figure 1b**). Positions of these bands are characterized by the so-called Jablczynski spacing coefficient $p = x_{n+1}/x_n \sim 1.04$ (**Figure 1c**) and their widths, w, are related by another well-known phenomenological power law, $q = p^k$, where $q = w_{n+1}/w_n$, $k \sim 0.9$-0.95, and q values are stable between $p^{0.9}$ and $p^{0.95}$ except for the initial and terminal bands (**Figure 1d**; for other trends, experiments in different geometries, etc., see SI, **Section S3**).

When the individual PP bands are cut from the gels and the gel is dissolved – without affecting the crystals – in DMF, the nature of these crystals can be established by PXRD. As summarized in **Figures 1e,f**, the first blurred precipitation band contains green-colored crystals of $Cu_2(OH)_3NO_3$, which exists in two different crystal forms (roualite and gerhardite) differing in the packing density of NO_3^- anions but having identical diffraction patterns. Subsequent two bands contain spherical crystallites few to tens of μm in diameter and exhibiting PXRD patterns corresponding to a mixture of $Cu_2OH(BTC)(H_2O)_n{\cdot}2nH_2O$ and $Cu(BTC{-}H_2)_2{\cdot}(H_2O)_2$ MOFs.[8] Finally, bands starting from the fourth one feature well-developed HKUST-1 crystals with surface areas ~1400 m^2/g (**Figure S3**). Their crystallinity increases with increasing band number, as evidenced by decreasing widths of XRD peaks.

Evolution of crystal shapes in space and in time. Remarkably, the crystals evolve both in space and in time (**Figure 2** and **Figures S14, S15**). Along the spatial coordinate, crystals in consecutive bands change from cubic, to truncated cubic, to truncated octahedral, and ultimately to octahedral. Over several days, however, the faces of these polyhedra gradually become concave (for cubes, truncated octahedra, and octahedra in **Figure 2**) or their corners are being "etched away" (for truncated cubes). After several days, the crystals can assume quite unusual morphologies such as the Czech hedgehogs from truncated octahedra (second-from-the-right image in the bottom row in **Figure 2**). The formation and evolution of these crystals can be rationalized by an interplay between surface-energy effects[9a] and coordination of Et_3N to Cu^{2+}. Specifically, when the initial bands are formed, the concentration of Et_3N is relatively low and under supersaturation conditions, Cu^{2+} and BTC^{3-} can rapidly nucleate small, cube-shaped HKUST-1 crystals (Fm-3m space group) exposing {100} faces of the underlying fcc lattice.[9b] After Cu^{2+} is locally depleted and needs to be diffusively resupplied, the relative concentration of Et_3N, which is not consumed to form crystals, becomes higher and can suppress supersaturation by coordinating Cu^{2+} ions.[9c] Under such conditions, nucleation in subsequent PP zones becomes slower (i.e., crystal growth is more equilibrated) allowing for the growth of larger crystals exposing lower-energy {111} faces.[9b] The closer to the ligand/Et_3N reservoir and the higher the concentration of Et_3N in the gel, the larger the sizes of the {111} faces – accordingly, crystals' shapes change from cubic, to truncated cubic, to truncated octahedral, to octahedral.

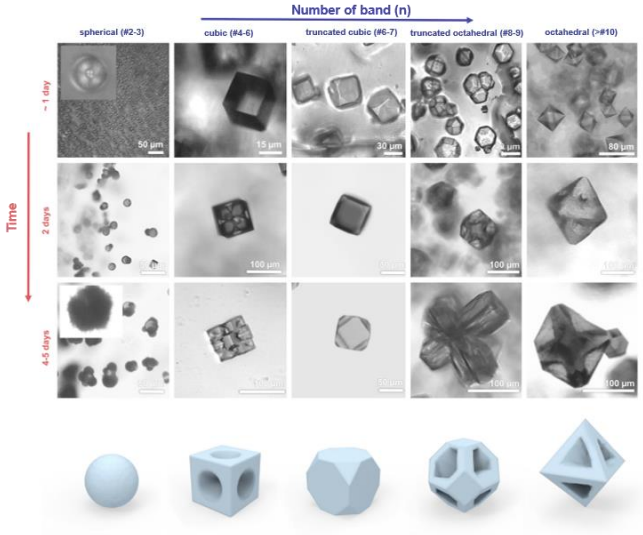

Figure 2. Evolution of MOF-crystal morphology in space and in time. Confocal microscopy images of crystals observed in consecutive PP bands (horizontal axis) and also changing in time (vertical axis). Spherical crystallites are assigned as $Cu_2OH(BTC)(H_2O)_n{\cdot}2nH_2O$ (ccdc #207414) and $Cu(BTC{-}H_2)_2{\cdot}(H_2O)_2$.[8] All polyhedral crystals are HKUST-1 crystals ($Cu_3(BTC)_2$; ccdc #112954). See corresponding PXRD spectra in Figure 1. The cartoons in the bottom row illustrate the etching of crystals' faces, evolving polyhedra into various concave shapes shown in experimental images. The so-called Czech hedgehogs (named so after Czech pre-WWII anti-tank obstacles) are second from the right in the bottom row.

After formation of the crystals, the concentration of Et_3N keeps increasing and its coordination to copper ions in the MOF results in crystals' etching. Interestingly, unlike in traditional inorganic crystals in which the high-free-energy regions are first to dissolve, MOFs can dissolve preferentially from the faces rich in metal-ligand bonds, as previously described by Avci *et al.* for ZIF MOF crystals.[9d] In the case of HKUST-1, {111} planes are lower in surface free energy than {100} faces, but the former planes have six Cu^{2+} base units per unit cell (paddle wheel $Cu_2(COO)_4$ secondary building units) exposed compared to only three in the {100} planes. Consequently, the {111} planes are etched first and the truncated cubes, truncated octahedra,

10.1002/anie.201910989

and octahedra shown in **Figure 2** evolve into "concave" structures. Of note, in cubic crystals observed in the initial PP bands, only {100} planes are exposed and so they are the planes being etched.

We emphasize that the full spectrum of crystal shapes and their homogeneity cannot be reproduced in solution-based experiments (see SI, **Section S6**). When the rate of delivery of Et_3N is carefully controlled, some trends of crystal growth are visible (e.g., change from cubes to octahedra upon increase in Et_3N concentration), but the sizes and morphologies of the microcrystals are inhomogeneous. Alternatively, when we followed the procedure of Sun's group[9b] and adjusted the effective concentrations of active species (especially the amount of the BTC^{3-} $3Et_3NH^+$ complex), we were able to reproduce the general succession of shapes seen in gels at short times, but the shape- and size purity of the samples was poor and the concavity of the faces was only marginal. Increasing the viscosity of the solution – to suppress any turbid flows and enhance diffusive transport – was also not successful, as only cubical and truncated cubical crystals were observed in concentrated sucrose and γ-cyclodextrin solutions. Unlike even very viscous solutions, in which growing crystals can still move freely/precipitate, gels hold them more "in place" ensuring they experience the same time-evolving concentration profile(s) of substrates and/or growth modifiers.

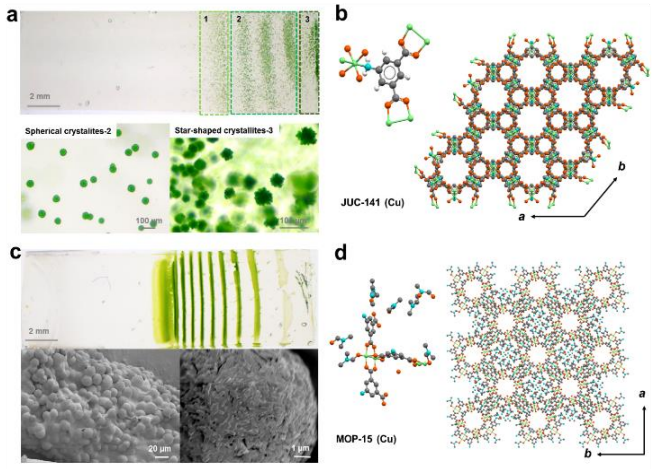

Figure 3. Periodic precipitation of MOFs and MOPs based on pH sensitive 5-NH_2-*m*BDC ligands. (a) A representative optical image of periodic bands obtained using Cu 5-NH_2-*m*BDC ligands at pH = 7.3. **(b)** Asymmetric unit of JUC-141 MOF (seen in central PP bands) and its Kagome lattice with the amino group of 5-NH_2-*m*BDC ligands coordinating to $Cu_2(COO)_4$ paddle wheel SBUs (the hexagonally arranged channels in the (001) direction are 12.3 Å in diameter). **(c)** Optical images of periodic bands emerging at pH = 9.84 along with SEM images of individual MOP-15 formations within these bands. **(d)** Diagrams of an asymmetric unit and packing structure of MOP-15. MOP-15's cage is cubohemioctahedral, has 24 terminal ligands and tetragonal symmetry (I4/m, *bcc* packing), and is held predominantly by hydrogen bonds. For experimental details and spectroscopic data, see SI, **Section 7**.

Extensions to MOPs and other MOFs. Similar phenomena are not limited to the HKUST-1 MOF and extend to other ligands and phases including metal-organic polyhedra, MOPs.[10a] For example, **Figure 3** illustrates outcomes of experiments in which the gel supported migration of $Cu_2(COO)_4$ paddle wheel secondary building units along with di-topic 5-amino-1,3-benzenedicarboxylic acid, 5-NH_2-*m*BDC, ligands and Et_3N. We surmised that in this system, crystallization and periodic precipitation might also depend perceptibly on the pH, as it influences the protonation/deprotonation equilibria of amino and carboxylic groups of the ligand (for pK_a's and titration curves, see SI, **Section S8**). Indeed, at low concentrations of Et_3N and pH below ca. 6.7, continuous/gradient rather than periodic precipitation is observed. Under these conditions, the amino groups (of both ligand and modulator) are protonated and the carboxylic acids are partly deprotonated such that the ligands cannot readily form extended 3D networks – instead, they form non-porous coordination polymers. Distinct PP patterns – characterized by spacing coefficients $p \sim 1.1$ and $q \sim 0.78$; SI, **Section S7** – are observed at higher Et_3N concentrations. In the pH = 6.8-9.2 range, the initial bands contain unidentified, irregularly shaped crystallites, followed by spherical crystals of JUC-141 MOF[10b] (kagome lattice and *eea* topology) in central bands, followed by star-shaped crystals of a non-porous coordination polymer. In contrast, above pH ~ 9.2, the same system gives PP bands comprised of spherical aggregates which are, in turn, composed of very small needle-like crystallites (visible on the SEM image in **Figure 3c**) with reflections consistent with those previously reported for MOP-15[10a, 10c] (though crystallinity is poor due to the presence of large amounts of water from the agarose matrix, as well as solubility of 5-NH_2-*m*BDCs in DMF used for gel-matrix digestion). For further examples (e.g., MOP-1 and MOP-OH systems) and additional discussion, see SI, **Section S9**).

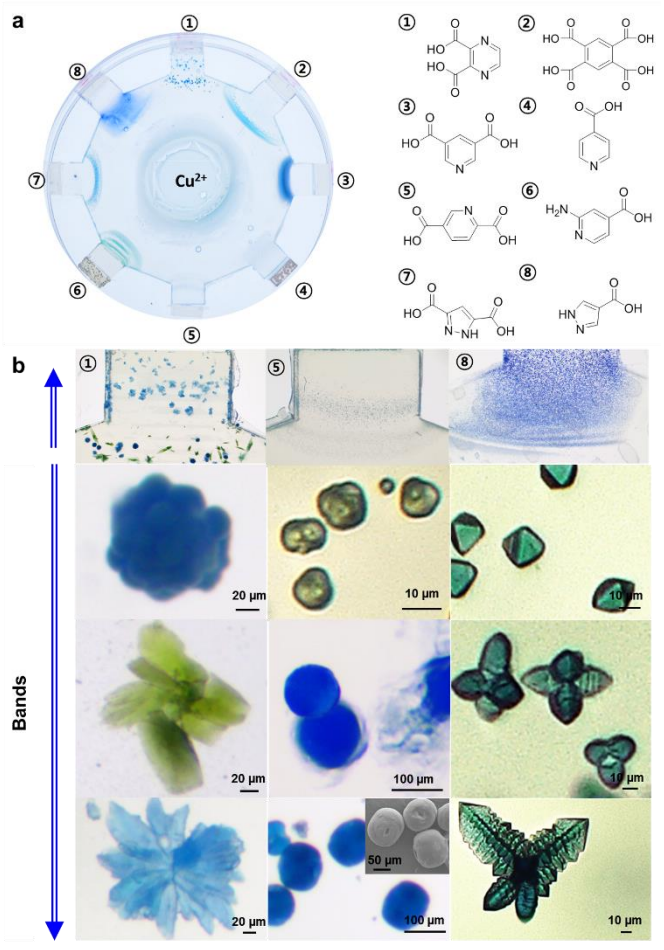

Figure 4. Extensions to other chemistries and parallelized PP arrangement. **(a)** Experimental image of a circular gel supporting eight reaction-diffusion processes involving centrally positioned reservoir of a metal salt (here, copper) and reservoirs of eight different ligands placed along the perimeter. Ligands' structures are shown on the right. **(b)** Three of the eight sub-systems illustrating variations in crystal sizes and morphologies. Inset in the middle column of the bottom row is a SEM image. For details, see main text and SI, Section 10.1.

We note that in studying (and screening for) similar PP systems, it is useful to parallelize the Wet-Stamping arrangement such that several types of RD processes – involving different metals and/or ligands – can proceed in various locations of the same gel. One

10.1002/anie.201910989

arrangement to do so is illustrated in **Figure 4a** whereby the reagents are delivered to the common gel substrate from (i) a centrally positioned gel carrying metal ions (e.g., 0.5 M $Cu(NO_3)_2$, 10 mL 1:1 v/v H_2O/EtOH), and (ii) multiple gel pieces placed around the perimeter and soaked with 0.1M H_2O/EtOH solutions of various carboxylate ligands and Et_3N. Although crystalline precipitates are observed for all ligands, only five systems, #1, #4, #5, #6, and #8 form PP patterns, underscoring that periodic precipitation requires proper timing between diffusion and crystal nucleation. **Figure 4b** shows images of crystallites collected from various bands of systems #1, #5, and #8 – these examples illustrate the richness of phases as well as variability of sizes and habits of crystals emerging from the PP processes (for details of these and other systems, see SI, Section 10.1). Specifically, in system #1, all bands contain crystallites of a CPL porous coordination polymer (2D MOF without pillar ligands) reported by Kitagawa's group[11]. These crystallites change from blue-colored, compact monoliths in the first precipitation band to a mixture of greenish rice-shaped and blue star-shaped particles in subsequent bands. In system #5, the first band contains spherical crystallites of Cu-PDC (pyridine-2,5-dicarboxylic acid) 1-D coordination polymer[12]. Within this first band, the sizes of the spheres gradually increase. From the second band onward, however, a new morphology appears as the aggregates become pumpkin-shaped with holes at their two poles (see SEM inset image in the bottom row of **Figure 4b**). In system #8, Cu-PyC (H_2PyC: pyrazole-4-carboxylic acid) forms an anionic MOF[13] (CCDC structure #891188). In the initial bands, the crystals are regularly shaped octahedra. Subsequently, however, crosses emerge in which the individual arms are tapered (which is unlike the HKUST-1 example from **Figure 2** where the arms were not narrowing outwards). With time and in higher bands, these arms develop smaller "teeth" pointing sideways, overall giving appearance of a fractal structure. We note that cross-like structures with highly textured arms are not observed without the use of Et_3N which, as we have seen before, coordinates to copper resulting in crystals' etching.

With further examples provided in the SI – including those of other metals, Co, Ni, Zn, or Cd (SI, **Sections S10.3-10.6**) and also those of hetermetallic MOFs prepared by diffusing ligands against sources of multiple metals (SI, **Section S11**) – we see the WETS platform as an enabling tool to produce spatially separated batches of MOF/MOP particles with well-controlled yet often unprecedented shapes not available to solution-based methods. Future research should consider system's scale-up (for practical applicability), addition of temperature control (to facilitate MOF growth at elevated temperatures), or transition to organogels (to extend the scope of suitable MOFs/MOPs).

Received:
Published online on:

Keywords: reaction-diffusion, periodic precipitation, metal-organic frameworks, metal-organic polyhedra, microcrystals

[1] a) I.R. Epstein, J.A. Pojman, *An Introduction to Nonlinear Chemical Dynamics: Oscillations, Waves, Patterns and Chaos*, Oxford University Press: New York, 1998; b) B. A. Grzybowski, K.J.M. Bishop, C.J. Campbell, M. Fialkowski, S.K. Smoukov, *Soft Matter* **2005**, *1*, 114-128; c) S. Soh, M. Byrska, K. Kandere-Grzybowska, B.A. Grzybowski, *Angew. Chem. Int. Ed.* **2010**, *49*, 4170-4198; d) I.R. Epstein, B. Xu, *Nat. Nanotechnol.* **2016**, *11*, 312-319.

[2] a) R.E. Liesegang, *Naturwissenschaftliche Wochenschrift*, **1896**, *11*, 353; b) Sultan, R. F. *Phys. Chem. Chem. Phys.* **2002**, *4*, 1253-1261; c) B. Chopard, M. Droz, J. Magnin, Z. Rácz, M. Zrinyi, *J. Phys. Chem. A* **1999**, *103*, 1432-1436; d) E. Nakouzi, O. Steinbock, *Sci. Adv.* **2016**, *2*, e1601144.e) P.J. Heaney, A.M. Davis, **1995**, *269*, 1562-1565; f) C.J. Campbell, E. Baker, M. Fialkowski, A. Bitner, S.K. Smoukov, B.A. Grzybowski, *J. Appl. Phys.* **2005**, *97*, 126102.

[3] a) M.E. Levan, J. Ross, *J. Phys. Chem.* **1987**, *91*, 6300-6308; b) S.C. Muller, J. Ross *J. Phys. Chem. A* **2003**, *107*, 7997-8008; c) I. Lagzi, *Langmuir* **2012**, *28*, 3350-3354; d) S.K. Smoukov, I. Lagzi, B.A. Grzybowski, *J. Phys. Chem. Lett.* **2011**, *2*, 345-349; e) R. Toth, R.M. Walliser, I. Lagzi, F. Boudoire, M. Duggelin, A. Braun, C. Housecroft, E.C. Constable, *Soft Matter* **2016**, *12*, 8367-8374; f) I. Bensemann, M. Fialkowski, B.A. Grzybowski, *J. Phys. Chem B* **2005**, 109, 2774-2778; g) S.K. Smoukov, A. Bitner, C.J. Campbell, K. Kandere-Grzybowska, B.A. Grzybowski, *J. Am. Chem. Soc.* **2005**, *127*, 17803-17807; h) J. Jiang, K. Sakurai, *Langmuir* **2016**, *32*, 9126-9134; i) B.A. Grzybowski, *Chemistry in Motion: Reaction-Diffusion Systems for Micro- and Nanotechnology*, John Wiley & Sons: Chichester, UK, 2009; j) I. Lagzi, B. Kowalczyk, B.A. Grzybowski, *J. Am. Chem. Soc.* **2010**, *132*, 58-60.

[4] a) R.Z. Douaihy, M. Al-Ghoul, M. Hmadeh, *Small* **2019**, *15*, 1901605; b) D. Saliba, M. Ammar, M. Rammal, M. Al-Ghoul, M. Hmadeh, *J. Am. Chem. Soc.* **2018**, *140*, 1812-1823; c) M. Al-Ghoul, R. Issa, M.Hmadeh, *CryeEngComm* **2017**, *19*, 608-612; d) R. Issa, M. Hmadeh, M. Al-Ghoul, *Def. Diff. Forum* **2017**, *380*, 39-47.

[5] a) Y.H. Wei, S.B. Han, D.A. Walker, P.E. Fuller, B.A. Grzybowski, *Angew. Chem. Int. Ed.* **2012**, *51*, 7435-7439; b) P.J. Wesson, S. Soh, R. Klajn, K.J.M. Bishop, T.P. Gray, B.A. Grzybowski, *Adv. Mater.* **2009**, *21*, 1911-1915.

[6] a) I. Stassen, N. Burtch, A. Talin, P. Falcaro, M. Allendorf, R. Ameloot, *Chem. Soc. Rev.* **2017**, 46, 3185-3241; b) Y.K. Kim, S.-M. Hyun, J.H. Lee, T.K. Kim, D. Moon, H.R. Moon, *Sci Rep*, **2016**, *6*, 19337; c) P. Sarawade, H. Tan, D. Anjum, D. Cha, V. Polshettiwar, *ChemSusChem.* **2014**, *7*, 529-535.

[7] C.V. McGuire, R.S. Forgan, *Chem Commun.* **2015**, *51*, 5199-5217.

[8] a) J. Chen, T. Yu, Z. Chen, H. Xiao, G. Zhou, L. Weng, B. Tu, D. Zhao, *Chem. Lett.* **2003**, *32*, 590-591; b) K.-J. Kim, Y.J. Li, P.B. Kreider, C.-H. Chang, N. Wannenmacher, P.K. Thallapally, H.-G. Ahn, *Chem. Commun.* **2013**, *49*, 11518-11520; c) Y. Mao, L. Shi, H. Huang, Q. Yu, Z. Ye, X. Peng, *CrystEngComm* **2013**, *15*, 265-270.

[9] a) G. Wulff., *Z. Kristallogr* **1901**, *34*, 449-530; b) Q. Liu, J.-M. Yang, L.-N. Jin, W.-Y. Sun, *CrystEngComm* **2016**, *18*, 4127-4132; c) H.-X. Lin, Z.-C. Lei, Z.-Y. Jiang, C.-P. Hou, D.-Y. Liu, M.-M. Xu, Z.-Q. Tian, Z.-X. Xie, *J. Am. Chem. Soc.* **2013**, *135*, 9311-9314.d) C. Avci, J. Ariñez-Soriano, A. Carné-Sánchez, V. Guillerm, C. Carbonell, I. Imaz, D. Maspoch, *Angew. Chem. Int. Ed.* **2015**, *54*, 14417-14421.

[10] a) H. Furukawa, J. Kim, N.W. Ockwig, M. O`Keeffe, O.M. Yaghi, *J. Am. Chem. Soc.* **2008**, *130*, 11650-11661; b) N. Zhao, F. Sun, P. Li, X. Mu, G. Zhu, *Inorg. Chem.* **2017**, *56*, 6938-6942; c) C. Serre, J. Pelta, *Chem* **2017,** *2*, 459-469.

[11] H. Sakamoto, R. Matsuda, S. Kitagawa, *Dalton Trans.* **2012**, *41*, 3956-3961.

[12] a) D. Min, S. S. Yoon, D.-Y. Jung, C. Y. Lee, Y. Kim, W. S. Han, S. W. Lee, *Inorg. Chim. Acta.* **2001**, *324*, 293-299; b) D. Saha, T. Maity, T. Dey, S. Koner, *Polyhedron* **2012**, *35*, 55-61.

[13] a) S. Su, Y. Zhang, M. Zhu, X. Song, S. Wang, S. Zhao, S. Song, X. Yang, H. Zhang. *Chem. Commun.* **2012**, *48*, 11118-11120.; b) Y. Han, K. Liu, M. A. Sinnwell, L. Liu, H. Huang, P. K. Thallapally, *Inorg. Chem.* **2019**, *58*, 8922-8926.

10.1002/anie.201910989

Reaction-Diffusion

Jun Heuk Park, Jan Paczesny, Namhun Kim, and Bartosz A. Grzybowski*

Shaping microcrystals of metal-organic frameworks by reaction-diffusion

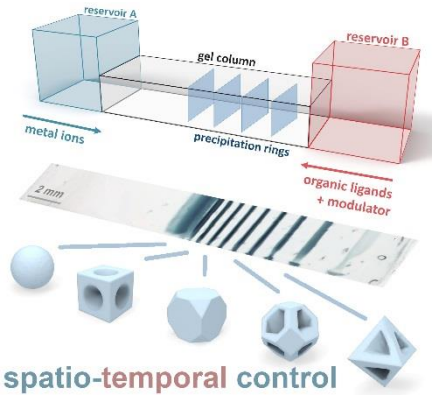

TOC TEXT: Reaction-diffusion process involving MOF or MOP components as well as a crystal-growth modulator yields periodic bands containing microcrystals that have different shapes and also evolve in time into unusual (e.g., concave) shapes.